

# Formation of Multiple-Satellite Systems From Low-Mass Circumplanetary Particle Disks

Ryuki Hyodo<sup>1</sup>, Keiji Ohtsuki<sup>1</sup> and Takaaki Takeda<sup>2</sup>

<sup>1</sup>Department of Earth and Planetary Sciences, Kobe University, Kobe 657-8501, Japan;

ryukih@stu.kobe-u.ac.jp, ohtsuki@tiger.kobe-u.ac.jp

<sup>2</sup>VASA Entertainment Co. Ltd.

Received \_\_\_\_\_; accepted \_\_\_\_\_

Not to appear in Nonlearned J., 45.

## ABSTRACT

Circumplanetary particle disks would be created in the late stage of planetary formation either by impacts of planetary bodies or disruption of satellites or passing bodies, and satellites can be formed by accretion of disk particles spreading across the Roche limit. Previous N-body simulation of lunar accretion focused on the formation of single-satellite systems from disks with large disk-to-planet mass ratios, while recent models of the formation of multiple-satellite systems from disks with smaller mass ratios do not take account of gravitational interaction between formed satellites. In the present work, we investigate satellite accretion from particle disks with various masses, using N-body simulation. In the case of accretion from somewhat less massive disks than the case of lunar accretion, formed satellites are not massive enough to clear out the disk, but can become massive enough to gravitationally shepherd the disk outer edge and start outward migration due to gravitational interaction with the disk. When the radial location of the 2:1 mean motion resonance of the satellite reaches outside the Roche limit, the second satellite can be formed near the disk outer edge, and then the two satellites continue outward migration while being locked in the resonance. Co-orbital satellites are found to be occasionally formed on the orbit of the first satellite. Our simulations also show that stochastic nature involved in gravitational interaction and collision between aggregates in the tidal environment can lead to diversity in the final mass and orbital architecture, which would be expected in satellite systems of exoplanets.

*Subject headings:* Moon – planets and satellites: formation – planets and satellites: dynamical evolution and stability – planet-disk interactions

## 1. Introduction

There are a variety of satellite systems in our solar system. The terrestrial planets have no or a small number (one or two) of satellites, while the giant planets have many. It is known that the systems of regular satellites of the giant planets have a common ratio of the total satellite mass to the host planet’s mass with  $\mathcal{O}(10^{-4})$  (e.g. Canup & Ward 2006). On the other hand, the satellite-to-planet mass ratio is as large as 0.012 and 0.1 for the Earth-Moon system and the Pluto-Charon system, respectively. Since processes of satellite formation are thought to be closely related to the formation process of the host planets, understanding of satellite formation is expected to provide constraints on planet formation.

The principal regular satellites of the gas giant planets are thought to be formed by accretion of solids in gas disks around forming host planets (e.g. Canup & Ward 2002, 2006, 2009; Estrada et al. 2009). For example, Canup & Ward (2006) showed that the common ratio between the total satellite mass and the host planet’s mass can be naturally explained by a balance between the supply of solids into the disk and the loss of formed satellites by inward migration to the planet due to the tidal interaction with the gas disk. Ogihara & Ida (2012) demonstrated that the configuration of the Laplace resonance among the inner three Galilean satellites can be explained when the existence of the disk inner edge is taken into account (see also Sasaki et al. 2010).

On the other hand, the Moon is thought to be formed by accretion from an impact-generated debris disk (Hartmann & Davis 1975; Cameron & Ward 1976). N-body simulation of lunar accretion from particulate disks showed that generally a single satellite is formed in a few months from initial disks of masses  $M_{\text{disk,ini}}/M_{\oplus} \simeq 0.02 - 0.05$  confined within the planet’s Roche limit (Ida et al. 1997; Kokubo et al. 2000), although the formation time scale becomes as long as  $\sim 10^2$  years if a hot fluid disk composed of vapor and melt is considered, because in such a case the rate of radial spreading of the disk and thus the growth rate of the satellite are controlled by the rate of radiative cooling of the

disk (Salmon & Canup 2012). Charon may also have been formed by accretion from an impact-generated debris disk, but impact simulations showed that it is more likely that Charon is an impactor that survived nearly intact (Canup 2005). In the above studies of satellite accretion from impact-generated disks, relatively massive initial particulate disks are necessary to account for the current total mass and angular momentum of the Earth-Moon or the Pluto-Charon system; the required disk mass ratio relative to the host planet is at least a few percent for the Moon, and more than 10% for Charon (Ida et al. 1997; Canup 2005).

On the other hand, Charnoz et al. (2010) considered satellite accretion from a circumplanetary particulate disk with a much smaller disk to host planet mass ratio to examine formation of moonlets around Saturn. Such a disk would have been formed either by tidal disruption of a passing comet (Dones 1991), disruption by meteoroid impact of a satellite that formed in the circumplanetary gas disk and migrated inward past the Roche limit (Charnoz et al. 2009), or tidal stripping of the outer layers of a migrating differentiated satellite in the circumplanetary gas disk (Canup 2010). When satellites are formed outside the Roche limit through radial diffusion of disk particles initially confined within the Roche limit, the mass of the formed satellite is larger when the disk surface density is larger, while the surface density gradually decreases due to the diffusion. As a result, satellites that were formed early in the evolution from a disk with a larger surface density are more massive. Also, the formed satellites migrate outward due to tidal interaction with the particle disk and the planet, but the tidal torques are increasing functions of mass. Consequently, more massive satellites migrate outward more rapidly, and these different migration rates lead to orbital crossings and merging. Charnoz et al. (2010) showed that the above mechanisms can explain the observed mass-orbital radius relationship among inner small moons of Saturn (i.e., their mass increases with increasing distance from Saturn), if radial spreading of a particle disk initially much more massive

than the current rings is considered.

Furthermore, Crida & Charnoz (2012) developed an analytic model for the accretion and orbital evolution of satellites from particulate disks with mass ratios relative to the host planet much smaller than the case of the lunar formation, and applied it to the formation of satellite systems of Saturn and other giant planets. Assuming that the disk surface density and the mass flux across the Roche limit are kept constant, Crida and Charnoz analytically investigated the growth and orbital evolution of formed satellites, and found that the observed relationship between the masses and orbital radii of regular satellites of Saturn, Uranus, and Neptune can be explained by their model. It should be noted that, in order to account for the current radial location of Saturn’s mid-sized moons including Rhea, the model by Crida & Charnoz (2012) (see also Charnoz et al. 2011) had to assume significantly strong tidal dissipation inside Saturn corresponding to the quality factor  $Q \sim 10^3$  as compared to the often assumed value of  $\sim 10^4$ , although there is a recent study that suggests such strong dissipation (Lainey et al. 2012).

The analytic model by Crida & Charnoz (2012) offers a unified understanding of the formation of satellite systems of terrestrial planets and those of giant planets. However, gravitational interaction between formed satellites is not taken into account in their model, which is expected to be important when formed satellites are massive, while previous N-body simulations of satellite accretion mostly focused on accretion of a single moon from relatively massive disks. On the other hand, using N-body simulation, Takeda (2002) investigated satellite accretion from particulate disks of various mass ratios to the host planet, and examined a relationship between the initial disk mass and the mass of formed satellites. Also, in order to examine the processes of the formation of the second satellite from the remaining disk after the formation of the first satellite, he performed simulations starting from a particulate disk with a satellite seed placed outside the Roche limit. However, direct N-body simulations of consecutive formation of multiple satellites

is desirable for better understanding of the whole accretion processes, including detailed orbital evolution of growing satellites and formation of co-orbital satellites during accretion.

Many exoplanets have been found so far, and the search for satellite systems of exoplanets is ongoing (e.g. Kipping et al. 2012, 2013a,b, 2014). Such satellites around exoplanets are also important in the context of astrobiology, because some of them would be located in the habitable zone. Thus, understanding of the formation processes of satellites from various particulate disks is important, not only for the understanding of the origin of satellite systems in our solar system, but also for those of exoplanets.

In the present work, we perform N-body simulations to investigate the process of consecutive formation of first and second satellites from particulate disks initially confined within the Roche limit. We examine how the masses of formed satellites depend on the initial disk mass, and also examine their orbital evolution in detail. In Section 2, we describe our numerical methods. Section 3 presents results for satellite accretion from massive disks similar to the case of lunar accretion, for comparison with results shown in later sections. Numerical results of the consecutive formation of first and second satellites from lighter disks are presented in Section 4. Section 5 discusses dependence on various parameters and diversity of satellite systems formed from particulate disks. Our results are summarized in Section 6.

## **2. The Model and Numerical Methods**

### **2.1. Initial Conditions**

We examine accretion of satellites from circumplanetary particle disks in a gas-free environment by performing global N-body simulation. Collision and gravitational interaction between particles are taken into account. As the initial condition, we consider

particle disks confined within the planet’s Roche limit given by

$$a_R = 2.456 \left( \frac{\rho}{\rho_c} \right)^{-1/3} R_c, \quad (1)$$

where  $\rho$  is the material density of particles, and  $\rho_c$  and  $R_c$  are the central planet’s density and radius, respectively. Initially, particles are distributed in an annulus with  $0.4a_R \leq r \leq a_R$ , and their surface density follows a power-law distribution  $\Sigma \propto r^\beta$ ; we examine cases with  $\beta = -1, -3$ , and  $-5$ . Initial orbital eccentricities and inclinations of particles are assumed to have small values that follow a Rayleigh distribution. In the following, we use the non-dimensional angular momentum of the disk given by

$$j_{\text{disk,ini}} = L_{\text{disk,ini}} / \sqrt{GM_c R_c}, \quad (2)$$

where  $L_{\text{disk,ini}}$  is the angular momentum of the initial disk, and  $M_c$  is the mass of the central planet. In the case of surface density distribution given above, we have  $j_{\text{disk,ini}} \simeq 0.83, 0.78$ , and  $0.73$  for  $\beta = -1, -3$ , and  $-5$ , respectively. We examine cases of various initial disk masses, with  $M_{\text{disk,ini}}/M_c = 0.01 - 0.06$ . The initial disks are described by  $3 \times 10^4$  to  $5 \times 10^4$  particles (Table 1).

We set the mass of the central planet to be the Earth’s mass and assume that the densities of the particles and the central planet are  $\rho = 3.3 \text{ g cm}^{-3}$  and  $\rho_c = 5.5 \text{ g cm}^{-3}$ , respectively, so that the case of massive disks corresponds to that of lunar accretion examined by previous works (Ida et al. 1997; Kokubo et al. 2000). However, evolution of self-gravitating particle disks is governed by their surface density rather than the density or mass of individual particles, and the mass of the initial disk relative to the planet ( $M_{\text{disk,ini}}/M_c$ ) and the initial angular momentum distribution of the disk are important parameters that control the outcome of satellite accretion (Ida et al. 1997; Kokubo et al. 2000; Takeda & Ida 2001). Also,  $R_c/a_R \simeq 0.34$  when the above values are assumed for the densities of the central planet and the particles, while we have  $R_c/a_R \simeq 0.4 - 0.5$  if the densities of the central planet and satellites corresponding to the gas giant planets

are assumed. However, as we show later, dynamical behavior near the disk outer edge is important for satellite accretion from a disk initially confined within the Roche limit (see also Ida et al. 1997; Kokubo et al. 2000). Therefore, our results can be applied to satellite accretion from particle disks in various cases, including ones around giant planets.

In our model, we assume a disk of condensed particles as the initial condition, but this may not be appropriate for massive disks. In fact, Salmon & Canup (2012) showed that vaporization of constituent particles would be important in the protolunar disk around the Earth when  $M_{\text{disk}}/M_{\oplus} \gtrsim 0.003$ , because in this case the amount of energy released during the viscous spreading of the disk is comparable to the latent heat of vaporization of silicate and the rate of radiative cooling from the disk surfaces is too small compared to the viscous heating rate. By generalizing their estimates to the case of particle disks around a central planet with mass  $M_c$ , we find that the amount of energy released during disk spreading is comparable to the latent heat of vaporization of silicate when  $M_c/M_{\oplus} \gtrsim 0.3$ . On the other hand, the rate of radiative cooling from the disk surfaces becomes smaller than the viscous heating rate when  $M_{\text{disk}}/M_{\oplus} \gtrsim 0.003 \times (M_c/M_{\oplus})^{-1/3}$ . If we compare the latter condition with the range of disk-to-planet mass ratios examined in the present work ( $0.01 \leq M_{\text{disk,ini}}/M_c \leq 0.06$ ), we find that vaporization would be important at least near the midplane even in the case of the lightest disk ( $M_{\text{disk,ini}}/M_c = 0.01$ ) when  $M_c/M_{\oplus} \gtrsim 0.03$ . Salmon & Canup (2012) showed that the time scales of disk spreading and satellite accretion become significantly longer when the fluid disk inside the Roche limit is considered. Also, because of the prolonged period of interaction with the fluid inner disk, the formed satellite tends to have a larger semi-major axis compared to the pure N-body simulations. However, other basic characteristics of the final outcomes were quite similar to those of pure N-body simulations. For example, they found that the relationship between the mass of the formed satellite and the initial disk angular momentum can be explained by the semi-analytic relationship derived from pure N-body simulations (Ida et al. 1997)



with the above revised estimate of the semi-major axis of the formed satellite. While we acknowledge the importance of vaporization, in the present work we will focus on disks of solid bodies, as a first step of full N-body simulation of the multiple-satellite system formation.

## 2.2. Numerical Methods

The orbits of particles are calculated by numerically integrating the following equation of motion,

$$\frac{d\mathbf{v}_i}{dt} = -GM_c \frac{\mathbf{x}_i}{|\mathbf{x}_i|^3} - \sum_{j \neq i}^N Gm_j \frac{\mathbf{x}_i - \mathbf{x}_j}{|\mathbf{x}_i - \mathbf{x}_j|^3}, \quad (3)$$

where  $\mathbf{x}_i$ ,  $\mathbf{v}_i$ , and  $m_i$  denote the position relative to the center of the planet, the velocity, and the mass of particle  $i$ , respectively, and  $G$  is the gravitational constant. We use the modified fourth-order Hermite scheme (Kokubo & Makino 2004) with shared time steps for the integration. Gravitational forces between particles and the planet are calculated using GRAPE-DR, which is a special purpose hardware for gravity calculation.

Collision between particles is taken into account, assuming that particles are smooth spheres with normal restitution coefficient  $\varepsilon_n = 0.1$ . Previous works show that dynamical evolution is hardly affected by  $\varepsilon_n$ , as long as  $\varepsilon_n < 0.6$  (e.g., Takeda & Ida 2001). For the search of colliding pairs, we adopt the octree method implemented in REBOUND (Rein & Liu 2012). When a collision is detected, velocity change is basically calculated based on the hard-sphere model (Richardson 1994). Particles that collide with the planet are removed from the system. When a collision between particles takes place outside the Roche limit, colliding particles can become gravitationally bound and form aggregates. Whether colliding pairs become gravitationally bound or not is judged by the accretion criteria that takes account of the tidal effect (Ohtsuki 1993; Kokubo et al. 2000); we calculate the energy for the relative motion of the colliding pair using their positions and

velocities, and the pair is regarded as being gravitationally bound when their centers are within their mutual Hill radius and the energy is negative (Kokubo et al. 2000). Gravitational aggregates formed outside the Roche limit can be tidally disrupted when they are scattered back inside the Roche limit by a forming satellite or another aggregate. In order to correctly describe such phenomena, we basically adopt the so-called rubble-pile model (Kokubo et al. 2000) for aggregates formed near the Roche limit, and follow the orbits of constituent particles.

However, if we adopt this method for all the bodies for the entire simulation, a large portion of computing time has to be used for resolving collisions among constituent particles that form aggregates, and it is difficult to handle long-term orbital integration of formed aggregates. On the other hand, as we will show below, a satellite formed by particle accretion near the disk edge gradually migrates outward due to gravitational interaction with the disk. Once the satellite migrates sufficiently far from the Roche limit, it does not need to be treated as a rubble-pile, because it will not be scattered back inside the Roche limit any more. Therefore, in the present work, for the largest and the second largest aggregates in the system, we adopt the following treatment for the merger of constituent particles into a single body. The conditions for this treatment are: (i) the aggregate (the largest or the second largest) is sufficiently massive, and (ii) the radial distance of its center of mass from the planet is sufficiently larger than  $a_R$  so that it is ensured that it does not enter the Roche limit any more. When both the above two conditions are satisfied, the aggregate is replaced by a single sphere that has the same mass and center-of-mass velocity as those of the aggregate and the density equal to that of the constituent particles,  $\rho$ . The critical values of the mass and semi-major axis for this treatment are determined empirically; typically, in the case of the first satellite, the critical mass corresponds to about 70% of its final mass (the final mass is estimated empirically from previous works on lunar accretion as well as our simulations with and without the above treatment; see Figure 11),

and the critical distance is about  $1.15a_R$ . When the newly formed body (satellite) further accretes other particles, the mass of the satellite is increased accordingly.

Each simulation is continued until the system reaches a quasi-steady state, although formed satellites continue slow outward migration after their formation. In the case of the formation of a single satellite from massive disks, simulations are typically continued for  $500T_K$  ( $T_K$  is the orbital period at  $r = a_R$ ). On the other hand, in the case of low-mass disks where the evolution of the system is slow, we continue our simulations for  $10^3T_K$ .

### 3. Formation of Single-Satellite Systems from Massive Disks

In this section, we present results in the case of satellite accretion from relatively massive disks with  $M_{\text{disk,ini}}/M_c \simeq 0.05$ , for comparison with the case of accretion from lighter disks discussed in later sections. Satellite accretion from such massive disks corresponds to previous N-body simulations of lunar formation (Ida et al. 1997; Kokubo et al. 2000).

Figure 1 shows an example of our simulation that corresponds to such a massive disk. As we described in Section 2, the outer edge of the initial disk is located at  $r = a_R$  (Figure 1,  $t = 0$ ; the number in each panel represents time in units of the orbital period  $T_K$  at the Roche limit). First, spiral structures develop in the disk due to its self-gravity ( $t = 5T_K$ ). Then, angular momentum is transferred through gravitational interaction between spiral arms, and those particles transferred outward past the Roche limit start forming gravitational aggregates ( $t = 17T_K$ ). The largest aggregate is replaced by a single body when it becomes massive enough and is sufficiently far from the Roche limit as a result of outward migration, as we described in Section 2.2 ( $t = 34T_K$ ). The formed satellite continues outward migration ( $t = 93, 495T_K$ ), while disk particles are scattered by the satellite and collide with the planet (Ida et al. 1997; Kokubo et al. 2000). At the end of the simulation, a single-satellite system was formed, with the mass of the remaining disk

being only about 24% of the satellite mass, or 0.3% of the planet mass.

Figure 2 shows the evolution of the mass and semi-major axis of the satellite in this case. We can see that the satellite grows rapidly when its orbit is near the Roche limit (i.e.,  $r/a_R \simeq 1 - 1.2$ ). The time scale of the evolution in the early stage is determined by the angular momentum transfer in the disk (Kokubo et al. 2000; Takeda & Ida 2001). The viscosity of self-gravitating particle disks can be written as

$$\nu = CG^2\Sigma^2/\Omega^3, \quad (4)$$

where the coefficient  $C$  depends strongly on the distance from the planet (Takeda & Ida 2001; Daisaka et al. 2001), and also weakly on the elastic properties of particles (Yasui et al. 2012). The time scale of the increase of the satellite mass in the early phase of its rapid growth ( $\simeq 10^2 T_K$ ) shown in Figure 2 is roughly consistent with the time scale of viscous evolution of the disk (Kokubo et al. 2000).

In the case of massive disks, formation of a single satellite is a typical outcome, but in some cases a second largest satellite is formed as a co-orbital satellite of the largest one. Kokubo et al. (2000) report that in about 10% of their simulations, a co-orbital satellite with mass larger than 20% of the largest one was formed. Figure 3 shows an example of our simulation that produced such a co-orbital satellite. In this case, the co-orbital satellite is moving in a tadpole orbit about the  $L_4$  Lagrangian point of the largest satellite, and it stayed in this orbit until the end of the simulation ( $t = 500T_K$ ). Figure 4 shows the evolution of the masses and the semi-major axes of the two satellites in this case. We find that the secondary satellite is captured into the tadpole orbit during the phase of rapid growth of the primary satellite, and is locked in such an orbit while it migrates outward with the primary satellite. Collision of such a co-orbital satellite onto forming satellites may have played an important role in the impact history of satellites (Jutzi & Asphaug 2011).

In Figure 3, an edge-on views is also shown for the panel for  $t = 33T_K$ . This panel shows a side-view of the secondary satellite before it is replaced by a single body, and we

can see that it has a radially elongated shape due to the tidal force. Such aggregates formed just outside the Roche limit have elongated shapes, and are locked in synchronous rotation. However, with increasing distance from the planet as a result of outward migration, the tidal effect weakens and aggregates tend to have rounder shapes (Karjalainen & Salo 2004). Since in our simulation the largest and the second largest aggregates that satisfy the conditions described in Section 2.2 are respectively replaced by a single body, we do not follow the change of satellite shapes in the course of outward migration.

## 4. Formation of Multiple-Satellite Systems

### 4.1. Formation of the Second Satellite

Next, we present results for accretion from lighter particle disks, where the second satellite is formed. In our simulations with  $j_{\text{disk,ini}} = 0.775$ , the second satellite was formed when  $0.015 \leq M_{\text{disk,ini}}/M_c \leq 0.03$  (Table 1). In the marginal case of  $M_{\text{disk,ini}}/M_c = 0.03$ , the second satellite was not formed in one simulation (Run-7), but it was formed in another simulation where initial conditions were generated using a different set of random numbers (Run-7b). On the other hand, in the case with  $M_{\text{disk,ini}}/M_c = 0.01$ , the evolution of the system was so slow that we had to stop the simulation before the second satellite was formed, although its formation is expected if we continue the simulation. Figure 5 shows time series of the evolution of the system in the case of  $M_{\text{disk,ini}}/M_c = 0.015$ . Initial evolution of the disk is similar to the case of more massive disks shown in Section 3. First, spiral structures are formed as a result of gravitational instability ( $t = 4T_K$ ). Since the critical wavelength of the instability ( $\lambda_c$ ) is proportional to the disk surface density, we find that there are a larger number of arms in the present case compared to the case shown in Figure 5 ( $t = 5T_K$ ). As a result, the mass of each aggregate formed from particles transferred outside the Roche limit, which is roughly proportional to  $\Sigma\lambda_c^2$  (Kokubo et al.

2000), is smaller compared to the case of more massive disks (compare Figure 5,  $t = 32T_K$  with Figure 1,  $r = 17T_K$ ). Also, since the surface density of the disk is smaller, the outward mass flux across the Roche limit is also smaller. Collisions between these aggregates outside the Roche limit produce the first satellite ( $t = 69T_K$ ), whose mass ( $\sim 0.002 \times M_c$ ) is smaller than the case of more massive disks. When this first satellite satisfies the conditions described in Section 2.2, it is replaced by a single sphere ( $t = 102T_K$ ).

After its formation, the first satellite gradually migrates outward via gravitational interaction with the disk, as in the case of more massive disks ( $t = 69, 102T_K$ ). On the other hand, particles near the disk outer edge are pushed inward by the satellite, and a gap is formed between the satellite and the disk outer edge ( $t = 102T_K$ ). The growth of the satellite almost stalls by this stage, but a significant amount of mass corresponding to 3.3 times the satellite mass remains in the disk. In the case of more massive disks shown in Section 3, the mass of the first satellite was so large that it gravitationally scatters most of disk particles to lead to collision with the planet. However, in the present case of the lighter disk, the first satellite is too small to scatter disk particles onto the planet. Instead, the satellite migrates outward significantly through gravitational interaction with the remaining disk, and then the disk outer edge also gradually expands ( $t = 565T_K$ ).

The torque from the satellite exerts on disk particles at resonant locations (Goldreich & Tremaine 1980), and there are a number of  $m : m - 1$  inner mean motion resonances with the first satellite between the orbit of the first satellite and the disk outer edge. Because of this resonant effect, particles cannot spread across the Roche limit immediately after the first satellite is formed and starts outward migration. However, these resonances vanish beyond the radial location of the 2:1 inner mean motion resonance, which is located at  $r_{2:1} = 0.63a_s$  ( $r_{2:1}$  is the radial location of the 2:1 inner mean motion resonance with the first satellite, and  $a_s$  is the semi-major axis of the first satellite). Therefore, when  $r_{2:1}$  becomes larger than  $a_R$  as a result of outward migration of the first satellite, particles

near the disk outer edge pile up outside the Roche limit and the accretion of the second satellite begins (Figure 5,  $t = 690T_K$ ; Goldreich & Tremaine (1978); Takeda (2002) ). As in the case of the first satellite, the second satellite is replaced by a single sphere when its radial location is sufficiently far from the disk outer edge (Figure 5,  $t = 986T_K$ ). Formation of the second satellite at the location of the 2:1 resonance with the first one was also found in some cases in the hybrid simulations of Salmon & Canup (2012), but they mostly focused on the case of the formation of single-satellite systems because they were primarily interested in the lunar formation.

#### 4.2. Orbital Evolution of the First and Second Satellites

Figure 6 shows the evolution of the mass and the semi-major axis of the first and the second satellites formed in the case of Run-10. The mass growth of the first satellite is similar to the case of the formation of a single satellite from more massive disks described in Section 3; it undergoes rapid growth just outside the Roche limit, then repels the disk outer edge and begins outward migration. In the present case, the time scale of the viscous evolution of the particle disk is longer because of the smaller disk surface density, thus the growth time scale of the satellite is also longer. On the other hand, the second satellite is formed from particles piled up near the 2:1 resonance with the first satellite, as mentioned above. Exactly speaking, the satellite seed, which is formed near the location of the 2:1 resonance with the first satellite, grows by accreting particles spreading from the disk outer edge, while the orbits of many of these particles are interior to the resonance location and have specific angular momentum smaller than that of the satellite seed. As a result, the specific angular momentum of the second satellite can decrease during its rapid growth, and its semi-major axis stays near the disk outer edge (Figure 6). When the second satellite becomes sufficiently massive to repel the disk outer edge, its growth stalls and outward

migration begins. Then the second satellite is captured into the 2:1 mean motion resonance with the first satellite. Since the angular momentum that the second satellite receives from the disk is partly transferred to the outer first satellite through resonant interaction (Peale 1986), the two satellites continue outward migration, with their radial locations being locked in the resonance.

A similar evolution can be found in other cases of the formation of two satellites from disks with different initial masses. Figure 7 shows results for two cases with slightly more massive disks than the case shown above, with the same initial non-dimensional angular momentum of the disk. Because of the larger surface density of the initial disks, the viscous evolution of the disk and satellite formation proceeds faster, but the general feature of the evolution is similar to the case shown in Figure 6. In the case of  $M_{\text{disk,ini}}/M_c = 0.025$  (Run-8) shown in the right panel of Figure 7, a co-orbital satellite whose mass is 7% of the first satellite is formed on the orbit of the first satellite. This small companion was captured into the tadpole orbit when the first satellite was still near the disk, and migrates outward together with the first satellite. Then, when the eccentricity of the first satellite grew significantly, its orbit became unstable and collided with the first satellite at  $t = 833T_K$ . Out of our four simulations where two satellites (excluding co-orbitals) were formed, capture of a co-orbital satellite by the first satellite was found in two cases (Runs 3 and 8), which suggests that the formation of co-orbital satellites would be more common than the case of satellite formation from more massive disks (Kokubo et al. 2000). In the other case (Run-3), the mass of the co-orbital satellite was 7% of the first satellite.

The first and the second satellites continue outward migration while their orbits are kept locked in the 2:1 mean motion resonance. In the present work, we do not examine their subsequent longer-term evolution in detail. If there is sufficient amount of mass still available in the disk when the second satellite migrates sufficiently far from the disk outer edge, viscous diffusion of the disk is expected to lead to the formation of the third and the



forth satellites (Crida & Charnoz 2012). On the other hand, when the first two satellites are rather massive and are locked in the 2:1 resonance during their outward migration, as in the case examined in the present work, orbital eccentricities of the two satellites can grow during their migration, which would influence their subsequent dynamical evolution. Figure 8 shows the evolution of the eccentricities of the satellites in the cases where two satellites were formed. The eccentricity of the first satellite before the formation of the second satellite is generally small. However, after the second satellite is formed and is locked into the 2:1 mean motion resonance, the eccentricity of the second satellite oscillates and takes on rather large values ( $0.1 - 0.25$ ), and the eccentricity of the first satellite increases accordingly ( $\sim 0.05$ ). For comparison, we performed three-body orbital integration for the two satellites and the planet but without disk particles. The initial conditions were taken from those at  $t = 800T_K$  of our Run-10, and the integration was continued for  $5000T_K$ . We confirmed that the eccentricities of the first satellite ( $0.02 - 0.04$ ) and that of the second satellite ( $0.1 - 0.13$ ) did not grow as large as the cases shown in Figure 8, which suggests that the interaction between the satellites and the disk as well as their migration play an important role for the eccentricity evolution of the satellites.

In the present work, sufficiently massive aggregates that migrated far from the disk edge are replaced by single spheres. However, if the eccentricity of the second satellite becomes so large that its peri-center gets inside the Roche limit, the satellite would undergo tidal disruption, which is not taken into account in our simulation after the satellites are replaced by single spheres. Figure 9 shows results of an additional simulation we performed to examine such effects<sup>1</sup>. The simulation is the same as Run-8 until the formation of the second satellite, but we did not replace it with a single sphere in the present case and continued treating it as a rubble pile. We find that the mass of the second satellite

---

<sup>1</sup>This case is not listed in Table 1.

grows after its formation and then decreases significantly; this is because the satellite gets inside the Roche limit after its eccentricity grows significantly, and it undergoes tidal disruption. After that, the fragments of the first-generation second satellite accrete again to form the second satellite of the second generation. Such a cycle of tidal disruption and re-accumulation would be repeated. Interestingly, a part of the fragments of the disrupted second satellite reach the orbit of the first satellite, and contribute to its additional growth. If the first satellite migrates sufficiently outward during such a cycle, the orbit of the second satellite would move outward and, eventually, its peri-center would avoid getting inside the Roche limit. In any case, orbital evolution of multiple-satellite systems is important to understand the final outcomes of satellite accretion from particle disks.

## 5. Dependence on the Mass and Angular Momentum of the Initial Disk

### 5.1. Disk Evolution and Formation of the First Satellite

Figure 10 shows the evolution of the mass and semi-major axis of the first satellite for various initial disk masses. From Figure 10(a) we confirm that more massive disks lead to more rapid evolution and produce more massive first satellites. In general, the satellite grows mostly during the early phase of rapid growth, and then its growth slows down. Figure 10(b) shows the plots of the evolution of the semi-major axis of the first satellite for the three cases out of the six shown in Figure 10(a). In all these cases, we can see that the satellite undergoes rapid growth when its semi-major axis is smaller than about  $1.2a_R$  by accreting particles spreading across the Roche limit. When the satellite grows large enough to repel the disk outer edge, its growth almost stalls. At this stage, its semi-major axis is about  $1.2 - 1.3a_R$ , and its outward migration is rather smooth afterwards.

## 5.2. Mass of the First Satellite

Figure 11 shows the plots of the mass of the first satellites as a function of the initial mass of the disk ( $j_{\text{disk,ini}} = 0.775$ ). We find that the dependence changes at  $M_{\text{disk,ini}}/M_c \simeq 0.03$ . In the case of massive disks that produce single-satellite systems, Ida et al. (1997) analytically showed from the conservation of mass and angular momentum that the satellite mass is proportional to the mass of the initial disk (see also Kokubo et al. 2000). In the derivation of this relationship, it is assumed that particles initially in the disk either accrete to form the satellite, collide with the planet, or escape from the system through gravitational scattering by the satellite, and that the disk does not remain at the final stage. Ida et al. (1997) and Kokubo et al. (2000) confirmed that their numerical results of N-body simulations agree well with the analytic relationship.

The dashed line in Figure 11 is the fit to our numerical results for  $M_{\text{disk,ini}}/M_c > 0.03$ , assuming that the satellite mass is proportional to the mass of the initial disk. We confirm that our results for the case of the formation of single-satellite systems agree well with this relationship as in the previous works. On the other hand, in the case of lighter disks with  $M_{\text{disk,ini}}/M_c < 0.03$ , a significant mass still remains in the disk after the formation of the first satellite, and the second satellite is formed from the remaining disk. Thus, the assumption of the complete depletion of the initial disk at the time of the formation of the first satellite that was made in the derivation of the above analytic linear relationship between the satellite mass and the initial disk mass is not valid anymore. In fact, in the case of such low mass disks, the dependence of the mass of the first satellite on the initial disk mass is found to be stronger, and the satellite mass is approximately proportional to the square of the initial disk mass. In this case, the accretion efficiency of incorporation of disk material into the satellite (Kokubo et al. 2000) decreases with decreasing disk mass.

On the other hand, satellite accretion from particle disks with much lower initial mass was studied by Crida & Charnoz (2012), as we mentioned before. They investigated

satellite accretion in the limit where the mass of the satellites accreted from the disk is negligible compared to the disk mass, and assumed that the disk surface density and the mass flow rate across the Roche limit are constant during satellite accretion. In this case, if we define the time scale of the viscous spreading of the disk with viscosity  $\nu$  as  $T_\nu \equiv a_R^2/\nu$ , the rate of outward mass flow across the disk outer edge can be written as  $F = M_{\text{disk}}/T_\nu$ . Using the expression of the viscosity for the self-gravitating collisional disks (Equation 4) and  $M_{\text{disk}} = \pi a_R^2 \Sigma$ , we then have

$$F = \pi C G^2 \Sigma^3 / \Omega^3. \quad (5)$$

In the model of Crida & Charnoz (2012), satellites (or satellite seeds) formed near the disk outer edge grow by directly accreting particles spreading from the disk outer edge when the satellites are still near the edge ("continuous regime"), or by capturing moonlets formed by accretion of such spreading particles when the satellites somewhat migrate outward ("discrete regime"). In both cases, the growth rate of the mass of the satellites ( $M_s$ ) is determined by the mass flow rate  $F$ , and we have

$$M_s \propto F \propto \Sigma^3 \propto M_{\text{disk}}^3. \quad (6)$$

Crida & Charnoz (2012) showed that the mass of the formed satellite at the end of the discrete regime is given by  $M_s/M_c \simeq 2200(M_{\text{disk}}/M_c)^3$ . These satellites continue outward migration due to torques from the particle disk and the planet, and grow further by mutual collisions in the course of the migration ("pyramidal regime").

In Figure 12, we compile the fitting results to our simulations as well as those of previous works for satellite accretion from massive disks (Ida et al. 1997; Kokubo et al. 2000) and from light disks (Crida & Charnoz 2012). As we mentioned above, in the case of the formation of single-satellite systems from massive disks, the disk is cleared out quickly due to gravitational scattering by the massive first satellite. In this case, the mass of the first satellite is proportional to the initial disk mass (Ida et al. 1997; Kokubo et al. 2000).

On the other hand, the assumption of a constant disk surface density seems to be reasonable when the mass of the formed satellites is much smaller than the disk mass. In this case, the mass of the satellites is proportional to the cube of the disk mass, as we have shown above. The case of the formation of the first and the second satellites in our simulation is intermediate between the above two cases. In this case, the mass of the first satellite is not large enough to clear out the remaining disk, while it is too massive to neglect its influence on the remaining disk; the mass of the disk significantly decreases as a result of the formation of the first satellite, and the disk outer edge is shepherded by the first satellite after its formation. As a result, the dependence of the mass of the first satellite on the initial disk mass becomes also intermediate between the above two cases.

### 5.3. Formation of the Second Satellite

In the case of the disks with non-dimensional angular momentum  $j_{\text{disk,ini}} = 0.775$  shown above, the second satellite was formed when  $0.015 \leq M_{\text{disk,ini}}/M_c \leq 0.03$ , while single-satellite systems are formed from more massive disks (Section 4). However, evolution of particle disks depends not only on the mass but also on the angular momentum distribution of the initial disk (Ida et al. 1997; Kokubo et al. 2000). Figure 13 shows results of a series of simulations where the mass and angular momentum of the initial disk are varied. The filled circles show the cases where the second satellite was formed, while the open circles represent the cases where single-satellite systems are formed. The open triangle indicates the marginal case where whether the second satellite is formed or not depends on the choice of random numbers for generating initial conditions. From Figure 13, we find a tendency that the critical mass of the initial disk that produces multiple satellites decreases with increasing angular momentum, indicating that higher angular momentum of the initial disk facilitates the formation of single-satellite systems. Figure 14 shows the dependence

of the mass of the first satellite on the disk angular momentum. When the disk angular momentum is larger and more mass is located in the outer part of the disk, particles in the disk can be transported outward across the Roche limit more easily, thus the mass of the first satellite tends to be larger. Such a massive first satellite easily clears out the remaining disk, and the second satellite cannot be formed. On the other hand, in the case of compact disks with smaller angular momentum, the outward mass flux across the Roche limit is rather small and the mass of the first satellite tends to be also small, which facilitates the formation of the second satellite.

#### 5.4. Mass of the Second Satellite

Figure 15 shows the mass of the second satellites together with that of the first satellites as a function of the initial disk mass. As we mentioned in Section 5.2, the mass of satellites produced from lighter disks tends to be smaller. At the time of the accretion of the second satellite, the mass and the surface density of the disk are smaller compared to the initial disk due to the formation of the first satellite. Therefore, the mass of the second satellite tends to be smaller than that of the first satellite.

On the other hand, as we mentioned above, the efficiency of incorporation of disk material into the first satellite decreases with decreasing disk mass in the case of the formation of multiple satellites. When the mass of the first satellite is much smaller than the initial disk mass, the mass of the remaining disk at the time of the formation of the second satellite is still similar to that of the initial disk. As a result, the mass of the second satellite formed from such a remaining disk becomes similar to that of the first satellite. From Figure 15, we can confirm that the difference between the masses of the first and the second satellites becomes smaller with decreasing mass of the initial disk. This is also consistent with Crida & Charnoz (2012), who considered the case with much lighter disks.

In this case, the mass of the formed satellite at the end of the discrete regime is given by  $M_s/M_c \simeq 2200(M_{\text{disk}}/M_c)^3$  as we mentioned above, which is constant as the disk mass is assumed to be constant.

### 5.5. On the Diversity in Final Outcomes

As we have shown above, the typical outcome of satellite accretion from massive particle disks is single-satellite systems, while multiple-satellite systems are produced from lighter disks. Also, when multiple satellites are formed, outer satellites tend to be more massive, because of a larger surface density of the disk at the time of accretion and/or as a result of outward migration and merger of formed satellites. In both cases of single- and multiple-satellite systems, co-orbital satellites can be formed occasionally.

On the other hand, dynamical evolution of self-gravitating particle disks inevitably involves stochastic nature arising from gravitational scattering between aggregates as well as their collisional disruption and subsequent re-accumulation, which can result in diversity in outcomes of disk evolution. As an example, Figures 16 and 17 show results of Run-7b; in this case, the parameter values of disk mass and angular momentum are the same as those assumed in Run-7 ( $M_{\text{disk,ini}}/M_c = 0.03$ ,  $j_{\text{disk}} = 0.775$ ), but a different set of random numbers are used to generate initial positions and velocities of particles. In the case of Run-7, only one satellite was formed. On the other hand, two satellites are formed in Run-7b; unlike the above-mentioned typical cases, the inner satellite is more massive than the outer one. Also, the two satellites are found to be locked in the 1:2 mean motion resonance.

This system with an inner larger satellite and an outer smaller one was formed in the following way. First, radial spreading of particles from the disk leads to the formation of a number of satellite seeds just outside of the Roche limit, and they grow through mutual collision and accretion. However, accretion efficiency between bodies in the strong tidal field

is not 100% (Ohtsuki 1993; Canup & Esposito 1995; Ohtsuki et al. 2013), and collision between gravitational aggregates can lead to complete or partial disruption (Karjalainen 2007; Hyodo & Ohtsuki 2014). In the case of  $M_{\text{disk,ini}}/M_c = 0.03$  shown in Figures 16 and 17, the mass of satellite seeds is significantly large. When such aggregates are disrupted by collision, they are often elongated due to the tidal effect and ejected particles are spread in a rather wide range of radial locations. Also, gravitational interaction between aggregates as well as between aggregates and dispersed particles leads to significant changes in semi-major axes and eccentricities of aggregates. In the case shown in Figure 16, a relatively massive aggregate (which eventually becomes the outer smaller satellite in the final state) undergoes collision with another aggregate, which leads to partial disruption of the colliding bodies (Figure 16,  $t = 29T_K$ ). The mass of the aggregate shows abrupt increase at the time of the collision, because the temporarily combined object is regarded as a single body (the green line at  $t \simeq 28T_K$  in Figure 17a). The largest remnant body produced by this collision and disruption has a rather large semi-major axis, and its eccentricity is also increased (the green line in Figures 17b, c). Then, at  $t \simeq 33T_K$  (Figure 16), another aggregate experiences scattering and partial disruption that leads to outward displacement, when the aggregate loses significant mass (the red line in Figures 17a, b). Then, this aggregate undergoes a close encounter with the aggregate that was scattered outward before, and the former is scattered inward to the vicinity of the outer edge of the disk ( $t \simeq 43T_K$ ; the red line in Figure 17b). Afterwards, this satellite seed grows by accreting particles spreading from the disk outer edge, and eventually becomes the largest satellite (Figure 16,  $t = 59,146T_K$ ; Figure 17a). During the growth of this largest satellite, particles located in the region exterior to the satellite’s orbit are scattered by the satellite to outer orbits, and then captured by the outer smaller satellite. Thus, the outer satellite grows significantly during this phase. When the mass of the inner satellite becomes large enough to shepherd the outer edge of the disk, the satellite begins outward migration. The radial distance between the inner larger satellite



and the outer smaller one gradually shrinks and, eventually, they get captured into the 1:2 mean motion resonance (see also Salmon & Canup 2012). Then they continue outward migration while being locked in the resonance. The eccentricity of the outer smaller satellite becomes large ( $\sim 0.2$ ) after it is captured into the resonance (the green line in Figure 17c). The eccentricity of the inner satellite is rather small initially, but it grows significantly in the course of the outward migration due to the resonant effect (the red line in Figure 17c).

In the above evolution, gravitational scattering between aggregates and their imperfect accretion at collision in the tidal environment plays an essential role in producing the final outcome that is different from the typical case. When the disk is not too light, as in the case shown above, those aggregates formed near the disk outer edge have significant mass, and gravitational scattering between them and their disruption plays an important role in delivering significant mass to the outer region, which facilitates formation of satellites with large orbits. Thus, stochastic nature of gravitational scattering and collisional disruption in the tidal field can lead to significant diversity in the final outcome of satellite accretion.

## 6. Summary

In the present work, using N-body simulations, we have investigated formation of satellites from particulate disks initially confined within the Roche limit. While the formation of single-satellite systems from massive disks was examined by previous N-body simulation (Ida et al. 1997; Kokubo et al. 2000), we have studied processes of the formation of multiple-satellite systems from low-mass disks in detail. When the mass of the particle disk is smaller, a larger number of particles have to be used in the simulation to resolve spiral structures created due to collective effects among particles, which plays an essential role in the disk’s dynamical evolution. Also, simulations for a longer period of time are required, because the time scale of the disk evolution becomes

longer with decreasing surface density of the disk. In order to solve these problems, we have adopted a new approach; we replace the largest and the second largest aggregates by a single sphere, respectively, when they become sufficiently massive and migrate outward sufficiently far from the disk outer edge. This approach allowed us to perform simulations of consecutive formation of the first and the second satellites from particle disks. Formation of multiple-satellite systems has been recently examined based on analytic and numerical models (Charnoz et al. 2010; Crida & Charnoz 2012), but gravitational interaction between satellites was not taken into account in these studies.

We found that single-satellite systems are formed from massive disks, while multiple-satellite systems are formed from lighter disks. In the case that the non-dimensional disk angular momentum  $j_{\text{disk,ini}} = 0.775$ , multiple-satellite systems were formed when  $M_{\text{disk,ini}}/M_c \leq 0.03$ , and we found that multiple-satellite systems are more likely to be formed from disks with smaller angular momentum. In the case of the formation of single-satellite systems from massive disks, previous studies showed that the mass of the formed satellite is proportional to the initial mass of the disk (Ida et al. 1997; Kokubo et al. 2000). On the other hand, the recent analytic study examined satellite accretion in the limit where the mass of the satellites accreted from the disk is negligible compared to the disk mass, assuming that the disk surface density and the mass flow rate across the Roche limit are constant during satellite accretion (Crida & Charnoz 2012). In this case, it has been shown that the mass of the satellites is proportional to the cube of the disk mass. Our simulations show that the mass of the first satellite in the case of the formation of two-satellite systems is approximately proportional to the square of the disk mass for  $0.01 \leq M_{\text{disk,ini}}/M_c \leq 0.03$ , which is intermediate between the above two cases. We also found that the second satellite is formed near the location of the 2:1 mean motion resonance with the first satellite. After the formation of the second satellite, the two satellites continue outward migration while being locked in the resonance (see also

Salmon & Canup 2012). When the eccentricity of the inner satellite grows significantly as a result of this resonant effect, its pericenter would get inside the Roche limit and the satellite would undergo tidal disruption, while it would avoid disruption if it migrates outward sufficiently far from the Roche limit before the eccentricity grows significantly. More detailed studies are required for the orbital evolution of multiple-satellite systems formed by accretion from particle disks. On the other hand, co-orbital satellites are occasionally formed on the orbits of the first satellite (Kokubo et al. 2000). Although we did not find formation of co-orbital satellites on the orbit of the second satellite, this is likely due to the resolution of our simulations. Our results suggest that the observed co-orbital satellites in the Saturnian satellite system may have formed during the accretion of the primary satellites. Also, collision of co-orbital satellites onto forming satellites may have played an important role in the impact history of satellites (Jutzi & Asphaug 2011).

In most cases of our simulations that produced two-satellite systems, the first satellite on the outer orbit was more massive than the second one that was formed later on the inner orbit, and the two satellites are locked in the 2:1 mean motion resonance, as mentioned above. However, our simulation also showed that accretion from particle disks can produce satellite systems significantly different from such a typical outcome, owing to the stochastic nature involved in gravitational interaction and collision between aggregates in the tidal environment (Section 5.5). Such effects may have played an important role in producing characteristics of the mass and orbital architecture of the satellite systems in our Solar System. They would also be important in the formation of satellite systems of exoplanets, thus more detailed studies are desirable.

We are grateful to Shigeru Ida for discussion and support. We also thank Sebastien Charnoz and Aurelien Crida for discussion, and Hiroshi Daisaka for valuable assistance and advice in using GRAPE-DR systems. This work was supported by MEXT/JSPS

KAKENHI. Part of numerical simulations were performed using the GRAPE system at the Center for Computational Astrophysics of the National Astronomical Observatory of Japan. Visualization of simulation results was performed in part using Zindaiji 3. One of the authors (R. H.) would like to dedicate this work with gratitude to Kazuki Sumi.

## REFERENCES

- Cameron, A. G. W., & Ward, W. R. 1976, *Lunar Sci. Abs.* 7, 120
- Canup, R. M. 2005, *Sci*, 307, 546
- Canup, R. M. 2010, *Natur*, 468, 943
- Canup, R. M., & Esposito, L. W. 1995, *Icarus*, 113, 331
- Canup, R. M., & Ward, W. R. 2002, *AJ*, 124, 3404
- Canup, R. M., & Ward, W. R. 2006, *Natur*, 441, 834
- Canup, R. M., & Ward, W. R. 2009, in *Europa*, ed. R. T. Pappalardo, W. B. McKinnon, & K. K. Khurana (Tucson, AZ: Univ. of Arizona Press), 59
- Charnoz, S., Morbidelli, A., Dones, L., & Salmon, J. 2009, *Icarus*, 199, 413
- Charnoz, S., Salmon, J., & Crida, A. 2010, *Natur*, 465, 752
- Charnoz, S., Crida, A., & Castillo-Rogez, J. C. et al. 2011, *Icarus*, 216, 535
- Crida, A., & Charnoz, S. 2012, *Sci*, 338, 1196
- Daisaka, H., Tanaka, H., & Ida, S. 2001, *Icarus*, 154, 296
- Dones, L. 1991, *Icarus*, 92, 194
- Estrada, P. R., Mosqueira, I., Lissauer, J. J., D’Angelo, G., & Cruikshank, D. P. 2009, in *Europa*, ed. R. T. Pappalardo, W. B. McKinnon, & K. K. Khurana (Tucson, AZ: Univ. of Arizona Press), 27
- Goldreich, P., & Tremaine, S. 1978, *Icarus*, 34, 240
- Goldreich, P., & Tremaine, S. 1980, *ApJ*, 241, 425

- Hartmann, W. K., & Davis, D. R. 1975, *Icarus*, 24, 504
- Hyodo R., & Ohtsuki, K. 2014, *ApJ*, 787, 56
- Ida, S., Canup, R. M., & Stewart, G.R. 1997, *Natur*, 389, 353
- Jutzi M., & Asphaug, E. 2011, *Natur*, 476, 69
- Karjalainen, R., & Salo, H. 2004, *Icarus*, 172, 328
- Karjalainen, R. 2007, *Icarus*, 189, 523
- Kipping, D. M., Bakos, G. A., Buchhave, L. A., Nesvorny, D., & Schmitt, A. 2012, *ApJ*, 750, 115
- Kipping, D. M., Forgan, D., Hartman, J., et al. 2013a, *ApJ*, 777, 134
- Kipping, D. M., Hartman, J., Buchhave, L. A., et al. 2013b, *ApJ*, 770, 101
- Kipping, D. M., Nesvorny, D., Buchhave, L. A., et al. 2014, *ApJ*, 784, 28
- Kokubo, E., Ida, S., & Makino, J. 2000, *Icarus*, 148, 419
- Kokubo, E., & Makino, J. 2004, *PASJ*, 56, 861
- Lainey, V., Karatekin, O., & Desmars, J. et al. 2012, *ApJ*, 752, 14
- Ogihara, M., & Ida, S. 2012, *ApJ*, 753, 60
- Ohtsuki, K. 1993, *Icarus*, 106, 228
- Ohtsuki, K., Yasui, Y., & Daisaka, H. 2013, *AJ*, 146, 25
- Peal, S., J. 1986, in *Satellite*, ed. Burns, J.A., & Matthews, M.S. (Univ. of Arizona Press), 159

- Rein, H., & Liu, S.-F. 2012, *A&A*, 537, A128
- Richardson, D. C. 1994, *MNRAS*, 269, 493
- Salmon, J., & Canup, R. M. 2012, *ApJ*, 760, 83
- Sasaki, T., Stewart, G. R., & Ida, S. 2010, *ApJ*, 714, 1052
- Takeda, T. 2002, Doctoral thesis, Tokyo Inst. Tech.
- Takeda, T., & Ida, S. 2001, *ApJ*, 540, 514
- Yasui, Y., Ohtsuki, K., & Daisaka, H. 2012, *AJ*, 143, 110

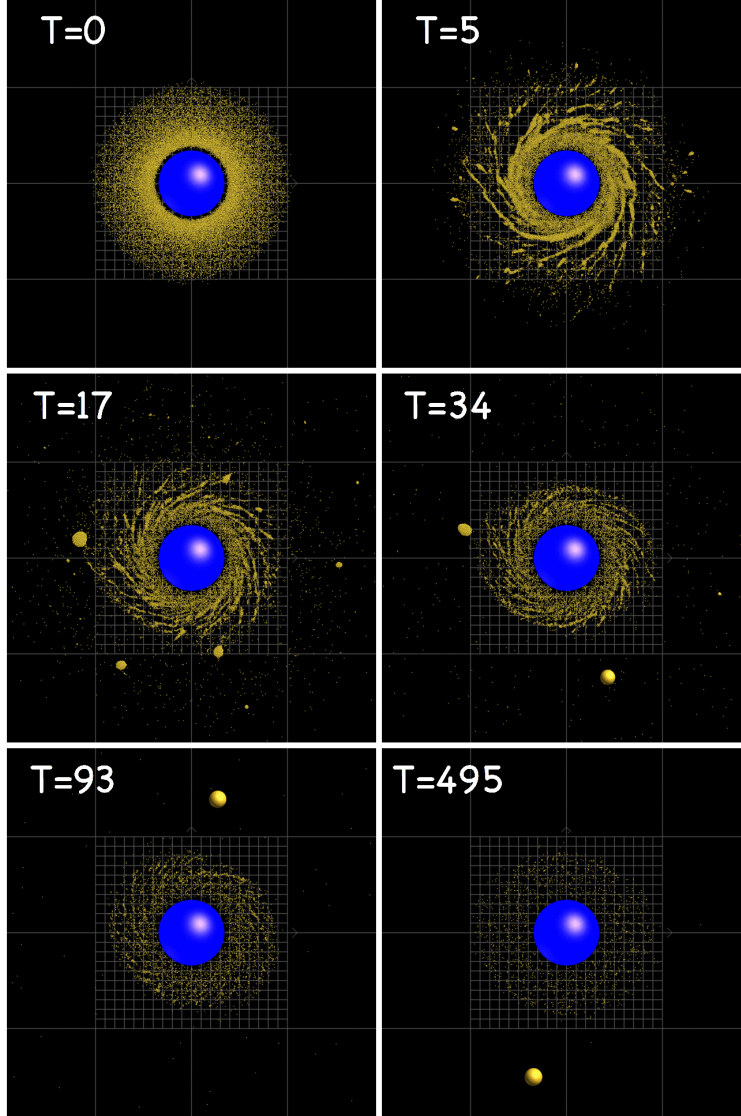


Fig. 1.— Snapshots of the simulation for the case of a single-satellite system (Run-4;  $M_{\text{disk,ini}}/M_c = 0.05$ ,  $j_{\text{disk,ini}} = 0.775$ ). Results are shown looking down onto the circumplanetary particle disk. Initially, the disk is confined in an annulus with  $0.4 \leq r/a_R \leq 1$ , while the radius of the central planet is  $R_c = 0.34a_R$ . Numbers in each panel represent the time elapsed since the start of the simulation, in units of the orbital period at the Roche limit.



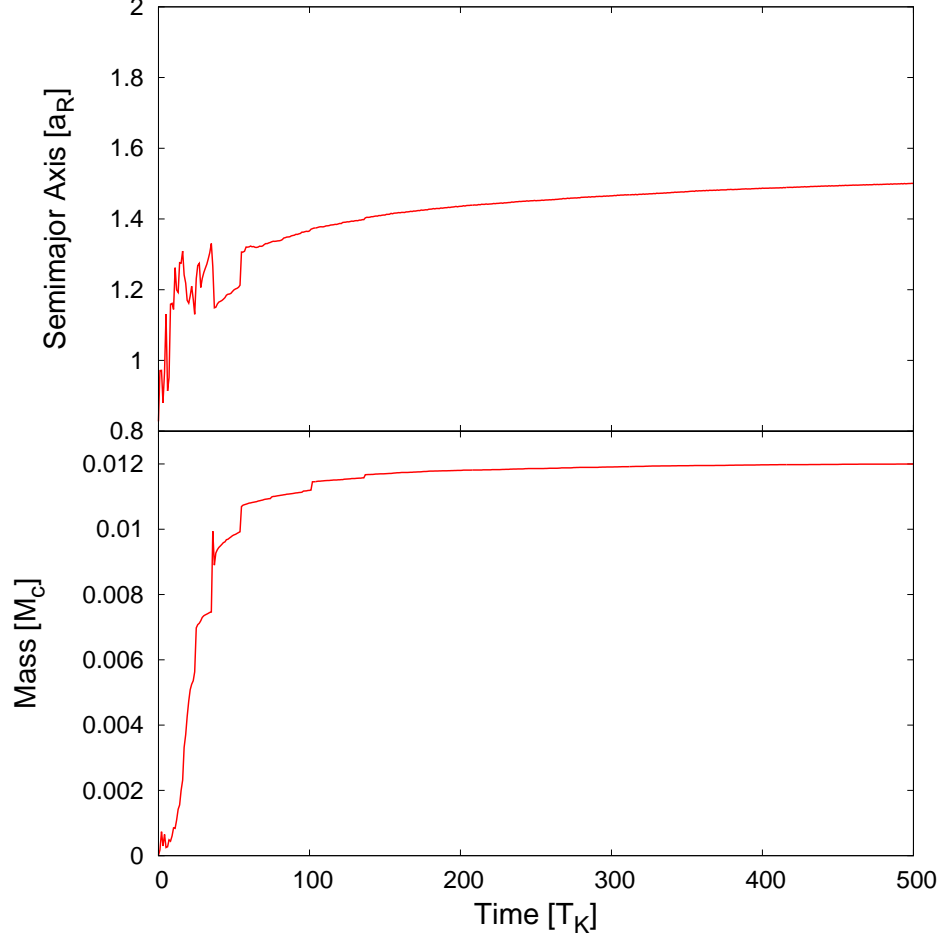


Fig. 2.— Evolution of the semi-major axis (top panel) and the mass (bottom panel) of the satellite in the case of Run-4 ( $M_{\text{disk,ini}}/M_c = 0.05$ ), where the final outcome is a single-satellite system.

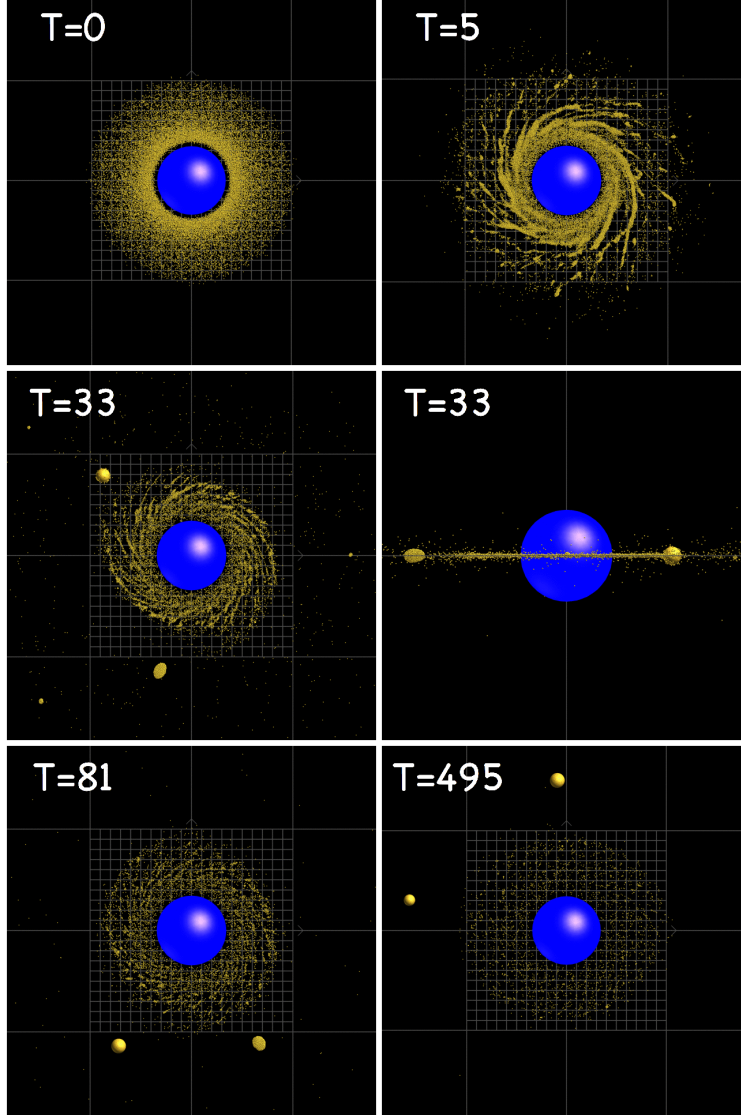


Fig. 3.— Snapshots of the simulation for the case where a system of a large satellite with a small co-orbital one was formed (Run-6;  $M_{\text{disk,ini}}/M_c = 0.04$ ,  $j_{\text{disk,ini}} = 0.775$ ). An edge-on view of the system is also shown for  $t = 33t_K$ , where we can see the radially elongated shape of the co-orbital satellite.

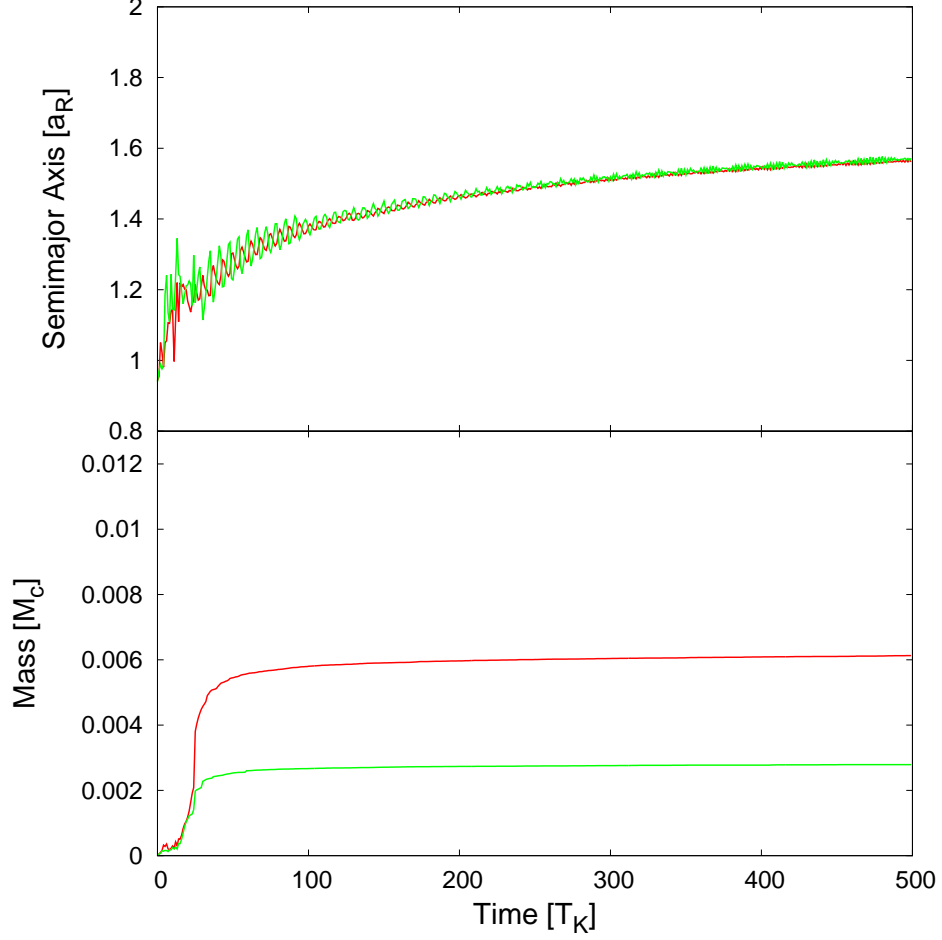


Fig. 4.— Evolution of the semi-major axis (top panel) and the mass (bottom panel) of the satellites in the case of Run-6 ( $M_{\text{disk,ini}}/M_c = 0.04$ ). The red lines represent those for the primary satellite, and the green lines represent those for the co-orbital satellite.

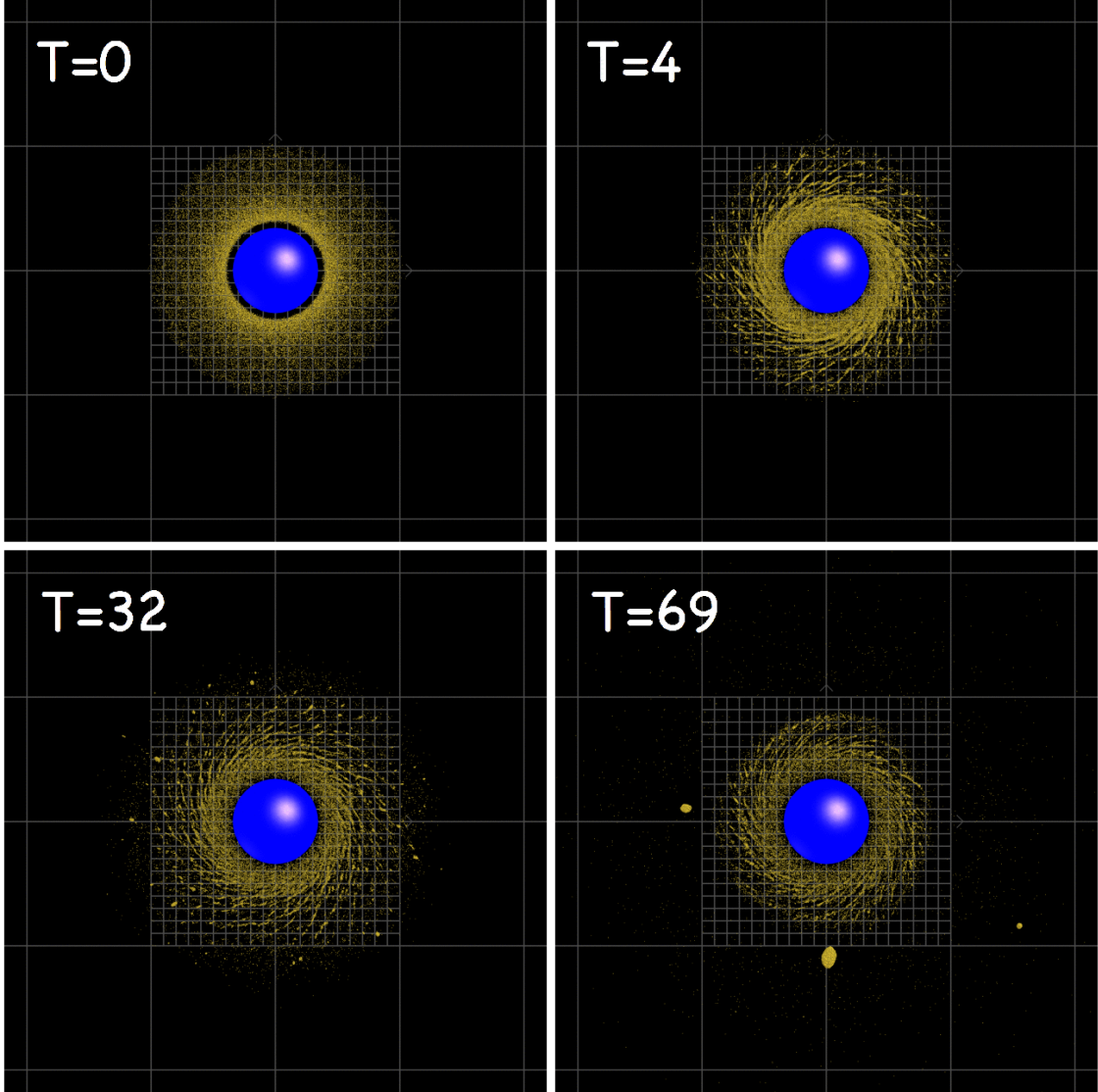


Fig. 5.— Same as Figure 1, but the case of the consecutive formation of two satellites is shown (Run-10;  $M_{\text{disk,ini}}/M_c = 0.015$ ,  $j_{\text{disk,ini}} = 0.775$ ).

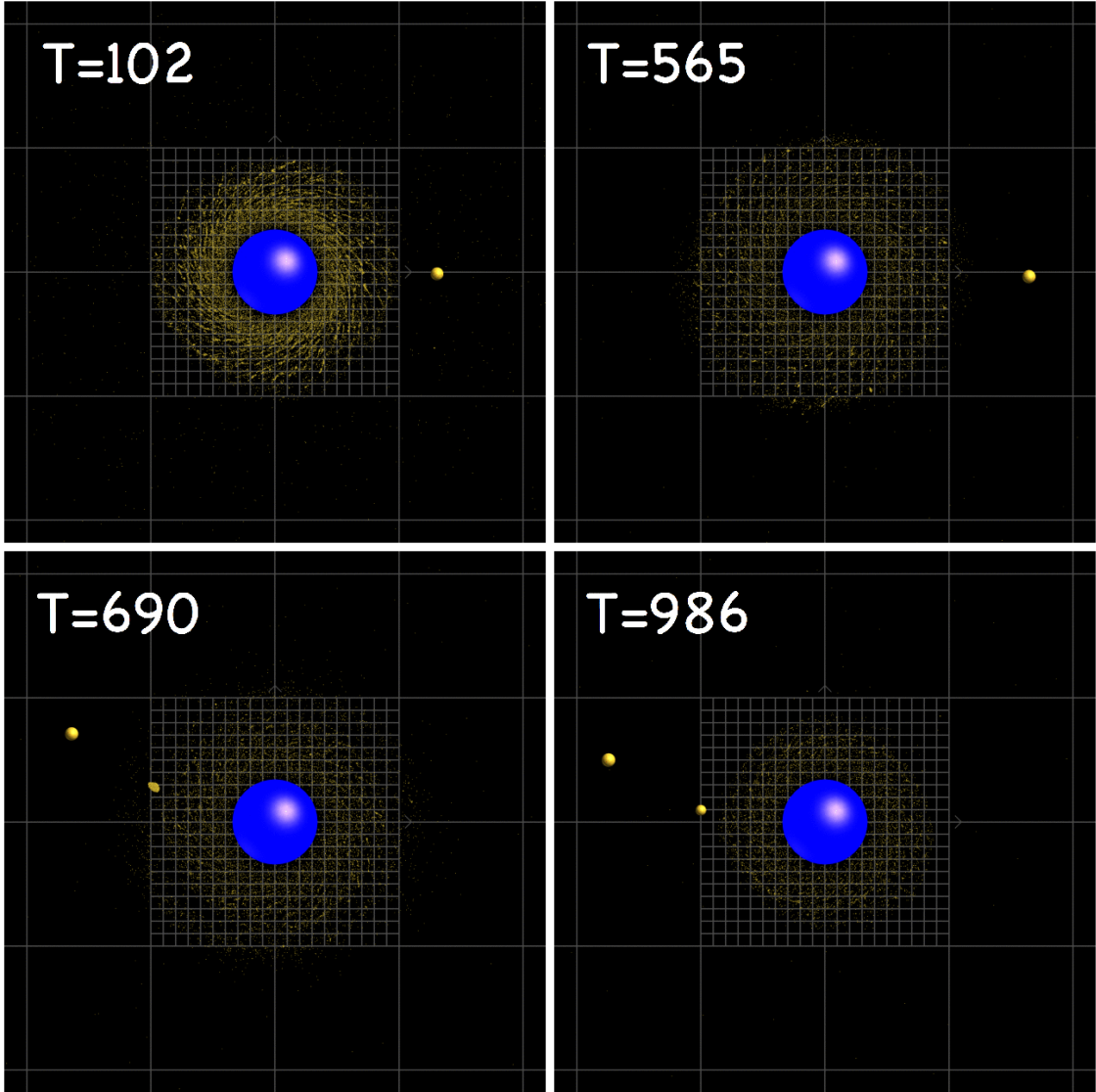


Fig. 5.— *Continued.*

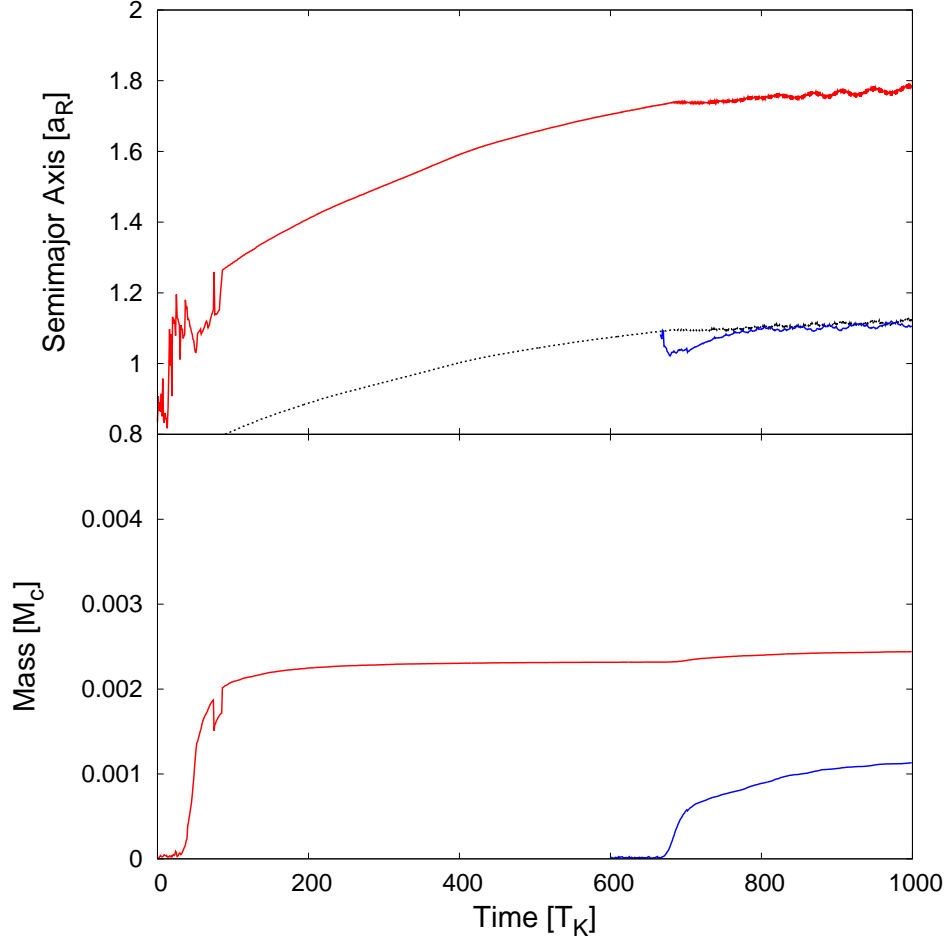


Fig. 6.— Evolution of the semi-major axis (top panel) and the mass (bottom panel) of the satellites in the case of Run-10 ( $M_{\text{disk,ini}}/M_c = 0.015$ ). The red lines represent the first satellite, and the blue lines represent the second one. The black dotted line in the top panel shows the radial location of the 2:1 mean motion resonance with the outer first satellite.

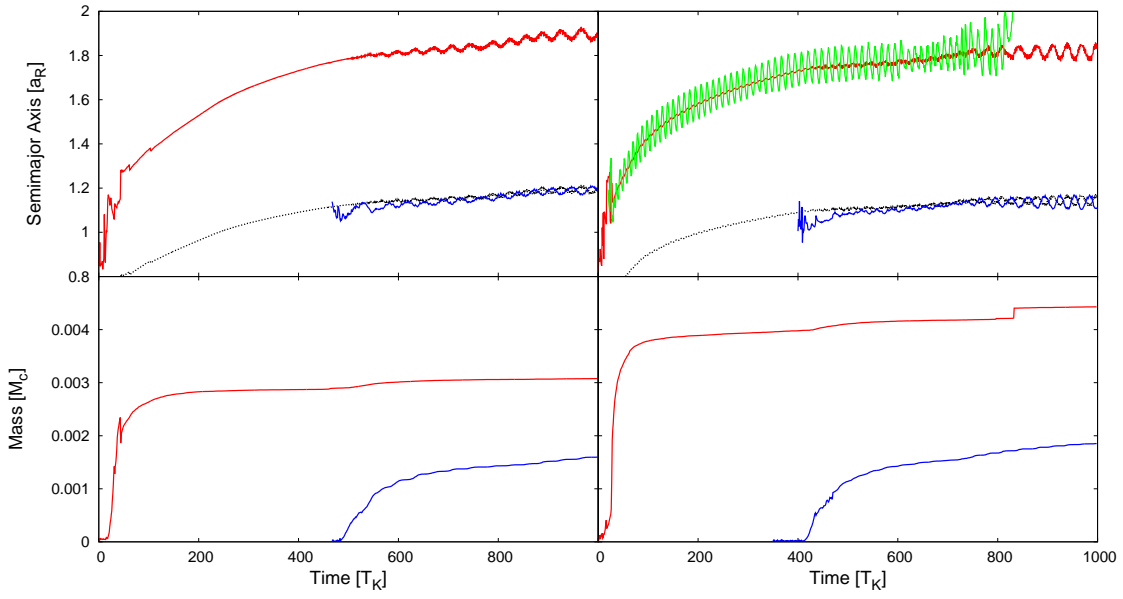


Fig. 7.— Same as Figure 6, but those for Run-9 ( $M_{\text{disk,ini}}/M_c = 0.02$ , left panel) and Run-8 ( $M_{\text{disk,ini}}/M_c = 0.025$ , right panel) are shown. In the case of Run-8, a co-orbital satellite was temporarily formed (green line), but it eventually collides and merges with the first satellite at  $t = 833T_K$ .

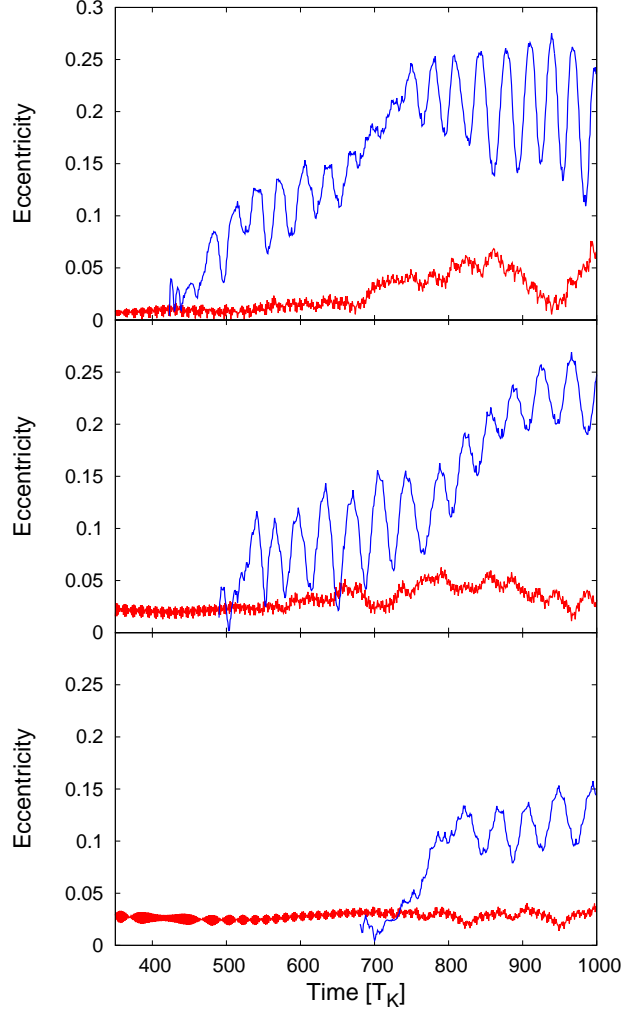


Fig. 8.— Evolution of the orbital eccentricity of satellites for Run-8 ( $M_{\text{disk,ini}}/M_c = 0.025$ , top panel), Run-9 (0.02, middle panel), and Run-10 (0.015, bottom panel). The red lines represent the first satellite, and the blue lines represent the second satellite.



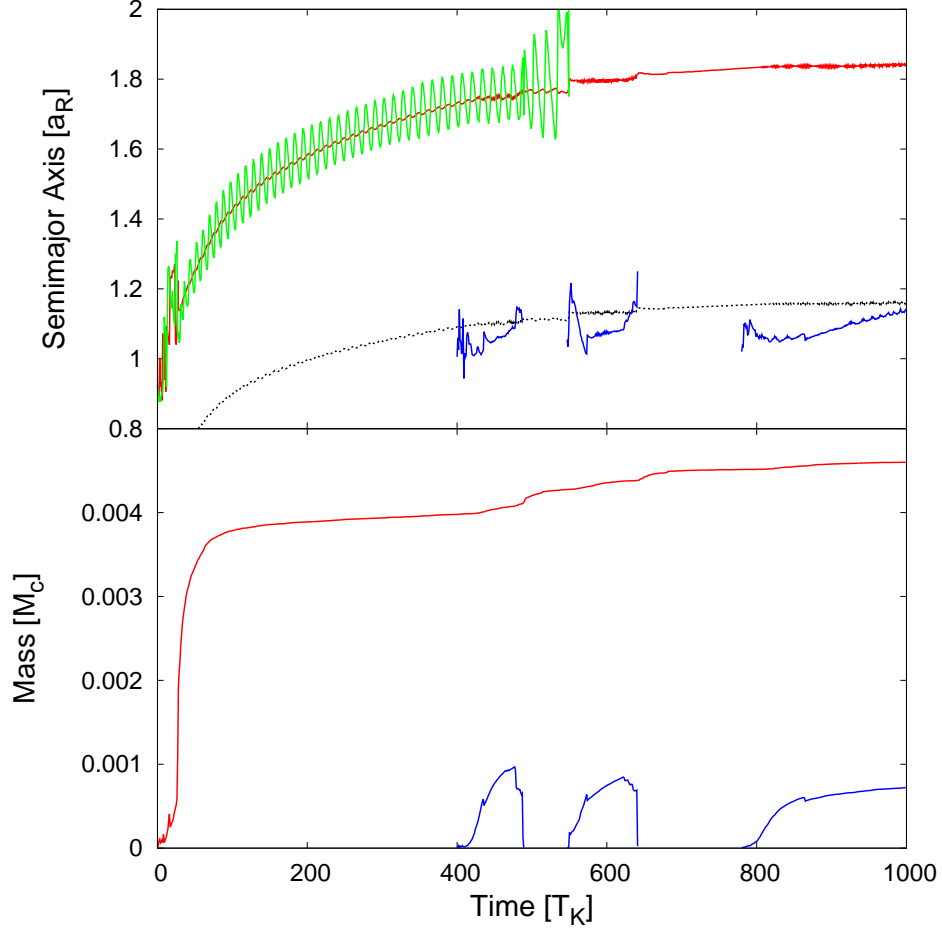


Fig. 9.— Evolution of the semi-major axis (top panel) and the mass (bottom panel) of the satellites in the case of the additional simulation, where the second satellite is treated as a rubble-pile object, without being replaced by a single sphere. Note that the simulation is the same as Run-8 shown in the right panel of Figure 7 until the formation of the second satellite. The meanings of the lines are the same as the right panel of Figure 7. In the present case, the co-orbital companion of the first satellite is scattered inside the Roche limit at  $t \simeq 550T_K$ .

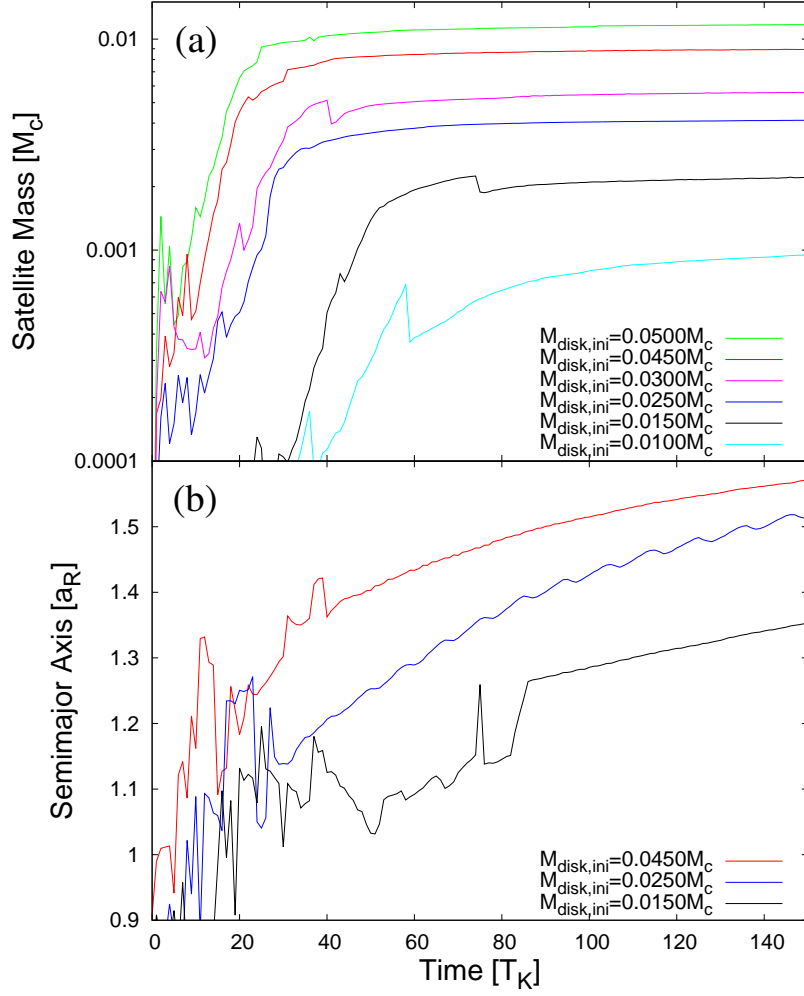


Fig. 10.— Evolution of the mass (top panel) and the semi-major axis (bottom panel) of the largest satellite in cases with various disk masses ( $j_{\text{disk,ini}} = 0.775$ ). In the top panel, the mass of the co-orbital companion on the orbit of the largest satellite as well as that of a small moonlet formed on an orbit exterior to the largest satellite’s orbit is added to that of the largest satellite to facilitate comparison.

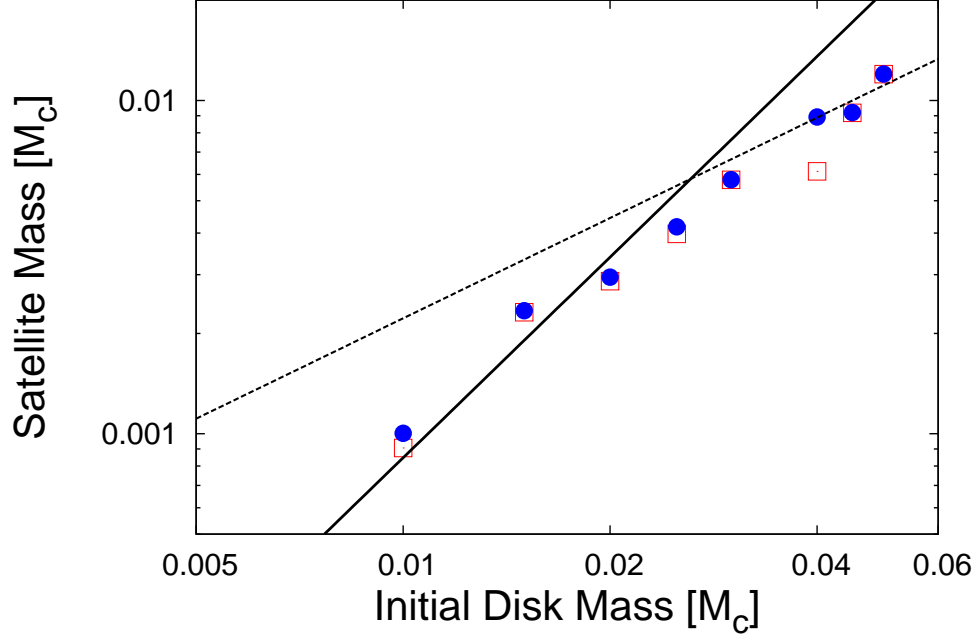


Fig. 11.— Mass of the first satellite as a function of the initial mass of the disk ( $j_{\text{disk,ini}} = 0.775$ ). Open squares represent the mass of the first satellite, while the filled circles show the sum of the masses of the first satellite and the second largest body in the system (i.e., a co-orbital satellite or a smaller satellite on an outer orbit). The dashed line represents the logarithmic fit to the numerical results for  $M_{\text{disk,ini}}/M_c > 0.03$  assuming that the satellite mass is proportional to the initial disk mass. The solid line is the logarithmic fit to the results for  $M_{\text{disk,ini}}/M_c < 0.03$ , assuming that the satellite mass is proportional to the square of the initial disk mass. The masses of the satellites in the case of the formation of single-satellite systems are those at the end of each simulation (i.e., those at  $t = 500T_K$ ), while those in the case of the formation of multiple-satellite systems are those just before the formation of the second satellite.

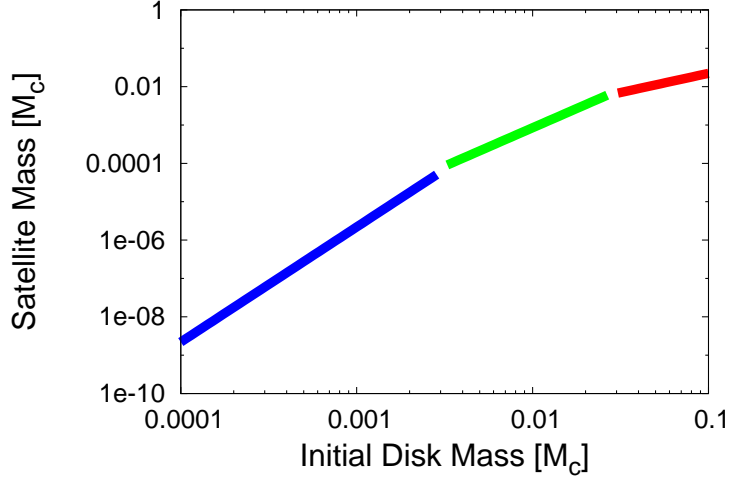


Fig. 12.— Dependence of the mass of the first satellite on the initial mass of the disk in three different regimes. The red line represents the case of the formation of single-satellite systems from massive disks, where the satellite mass is proportional to the disk mass. The green line represents the case of the formation of two-satellite systems, where the satellite mass is approximately proportional to the square of the disk mass. These two lines were obtained by logarithmic fits to our numerical results (Figure 11). Typical results of the previous N-body simulation of lunar accretion from massive disks fall within the width of the red line (i.e.,  $0.15 \lesssim M_s/M_{\text{disk,ini}} \lesssim 0.35$  for  $0.7 \lesssim j_{\text{disk,ini}} \lesssim 0.85$ ; Kokubo et al. (2000)), while our numerical results for the formation of two-satellite systems fall within the width of the green line (Figure 11). The blue line shows the result of Crida & Charnoz (2012) on the mass of the satellite formed at the end of the discrete regime (i.e.,  $M_s/M_c \simeq 2200(M_{\text{disk}}/M_c)^3$ ). Although they assume that the disk surface density is constant, actual disks should have surface density distribution, and the mass of satellites accreted from such light disks should also depend on the surface density (or angular momentum) distribution similarly to the numerical results in the other two regimes. Note that actual transitions between the regimes are expected to be rather smooth.

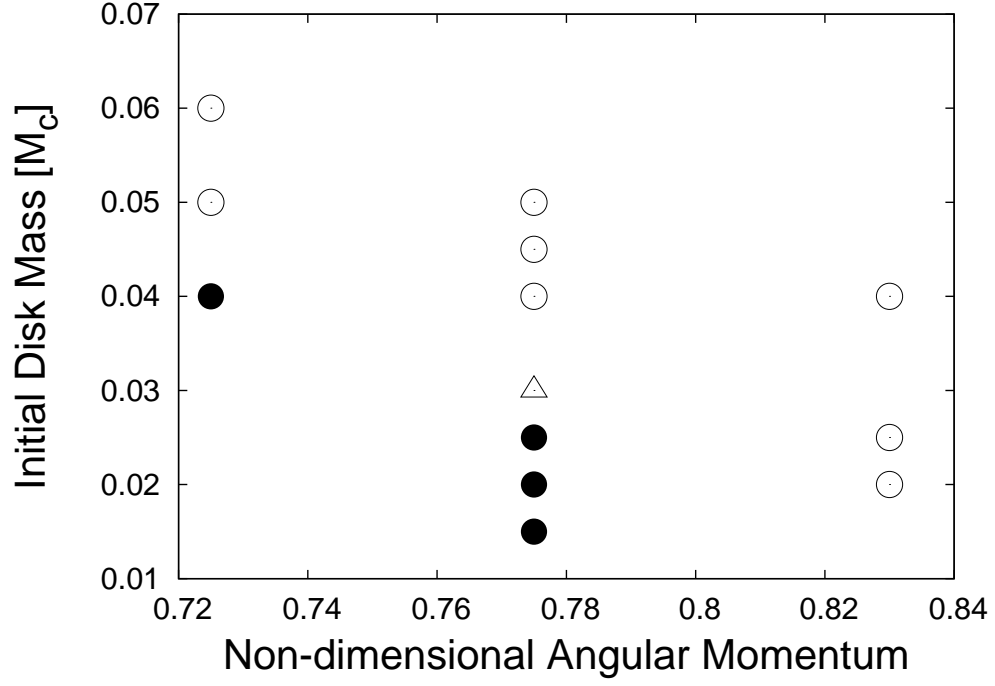


Fig. 13.— Outcomes of simulations with various values of initial disk mass and non-dimensional angular momentum of the disk. Filled circles indicate the case where the second satellite is formed, while open circles represent the case that results in single-satellite systems. Open triangle shows the marginal case where whether the second satellite is formed or not depends on the choice of random numbers for generating initial positions and velocities of particles.

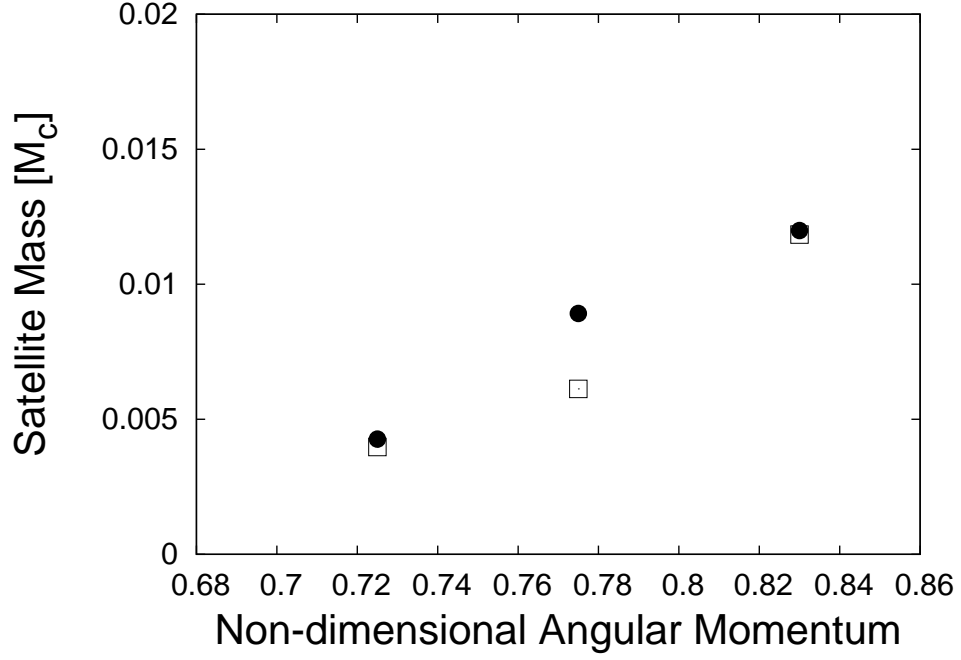


Fig. 14.— Dependence of the mass of the first satellite on the non-dimensional angular momentum of the initial disk (Runs 3, 6, and 12;  $M_{\text{disk,ini}}/M_c = 0.04$  in all the three cases). Open squares represent the mass of the first satellite, while the filled circles show the sum of the masses of the first satellite and the second largest body in the system (i.e., a co-orbital satellite or a smaller satellite on an outer orbit).

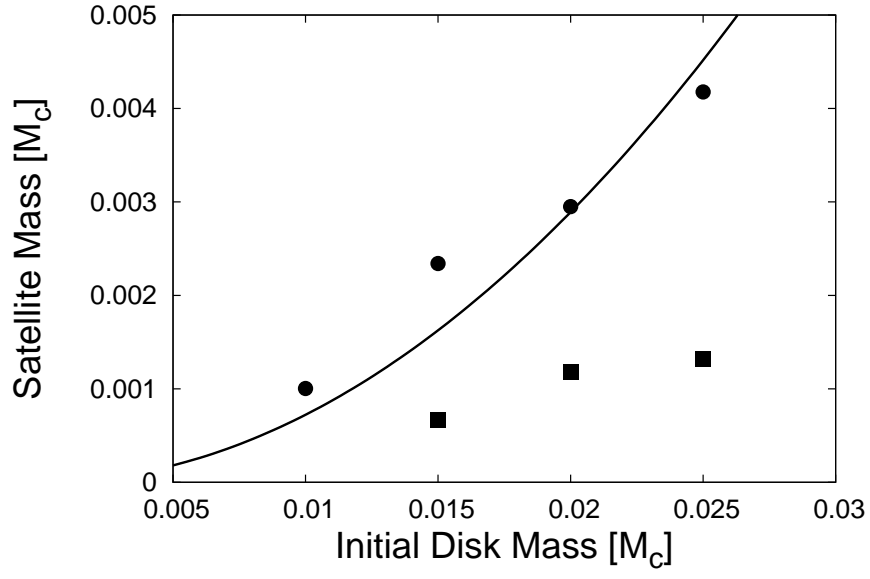


Fig. 15.— Mass of the first satellite (circles) and the second satellite (squares) as a function of the initial mass of the disk ( $j_{\text{disk,ini}} = 0.775$ ). The solid line represents the fit to the results for the first satellite, assuming that the satellite mass is proportional to the square of the initial disk mass.

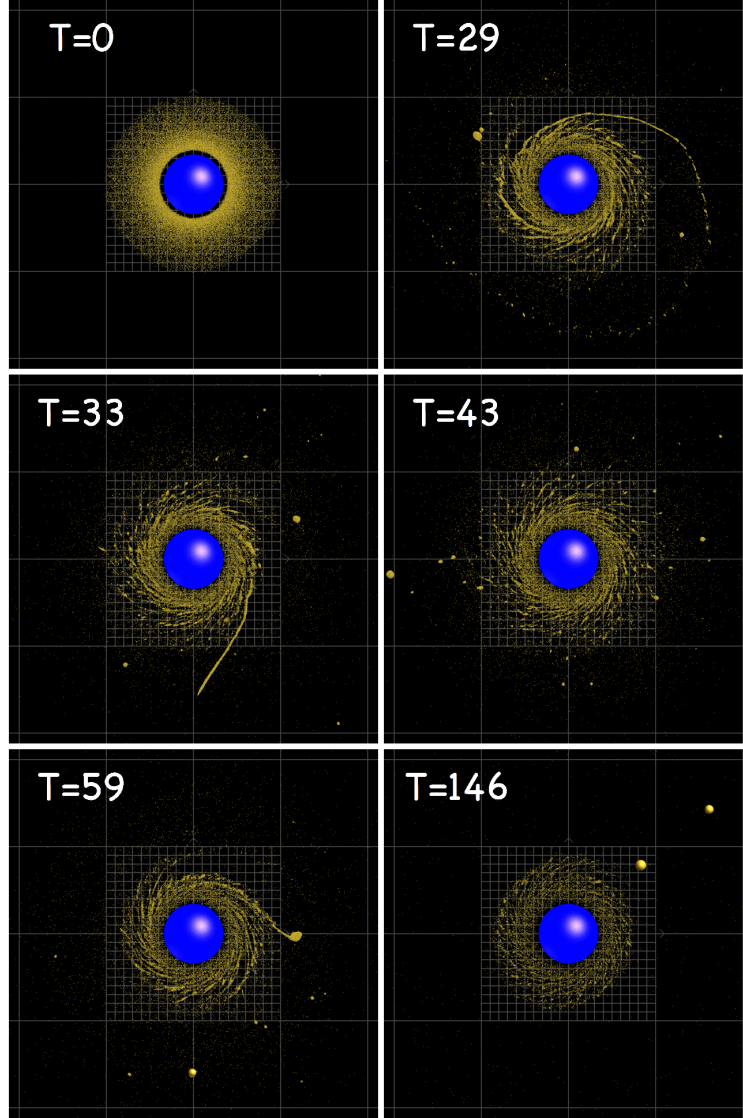


Fig. 16.— Snapshots of the simulation for the case of the formation of the two-satellite system with a larger satellite on an inner orbit and a smaller one on an outer orbit (Run-7b;  $M_{\text{disk,ini}}/M_c = 0.03$ ,  $j_{\text{disk,ini}} = 0.775$ ).



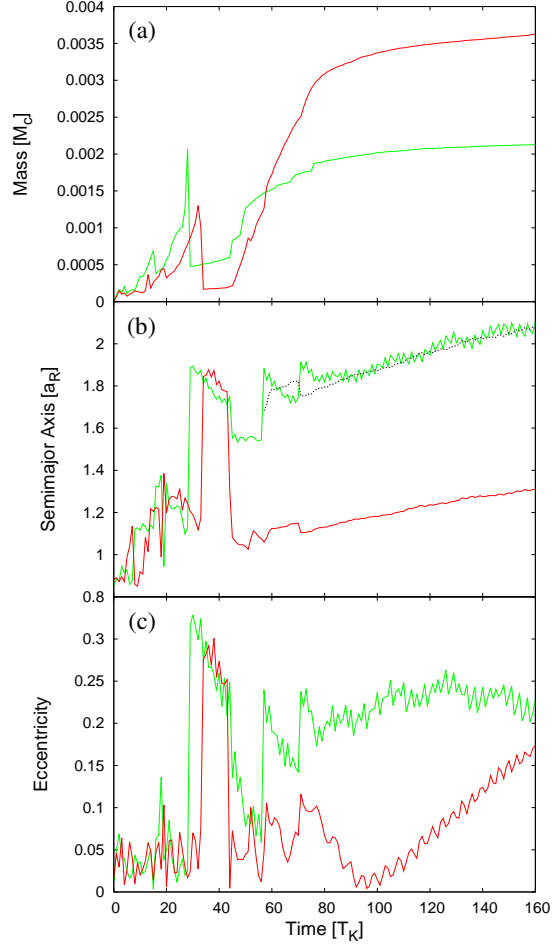


Fig. 17.— Evolution of the mass (top panel), semi-major axis (middle panel), and eccentricity (bottom panel) of the satellites in the case of Run-7b shown in Figure 16. The red lines represent the one that eventually becomes the largest satellite on an inner orbit, and the green lines represent the one that becomes the smaller satellite on an outer orbit. The black dotted line in the middle panel shows the radial location of the 1:2 mean motion resonance with the inner largest satellite.

Table 1: Initial Disk Parameters and Mass of Formed Satellites

Run	$M_{\text{disk,ini}}/M_c$	$j_{\text{disk,ini}}$	$N$	$M_{\text{s,out}}/M_c$	$M_{\text{s,in}}/M_c$
1	0.060	0.725	30,000	$8.72 \times 10^{-3}$	...
2	0.050	0.725	30,000	$7.98 \times 10^{-3}$	...
3	0.040	0.725	50,000	* $4.27 \times 10^{-3}$	$2.43 \times 10^{-3}$
4	0.050	0.775	30,000	$1.20 \times 10^{-2}$	...
5	0.045	0.775	30,000	$9.18 \times 10^{-3}$	...
6	0.040	0.775	30,000	* $8.92 \times 10^{-3}$	...
7	0.030	0.775	50,000	$5.78 \times 10^{-3}$	...
7b	0.030	0.775	50,000	$2.13 \times 10^{-3}$	$3.63 \times 10^{-3}$
8	0.025	0.775	50,000	* $4.18 \times 10^{-3}$	$1.32 \times 10^{-3}$
9	0.020	0.775	50,000	$2.87 \times 10^{-3}$	$1.18 \times 10^{-3}$
10	0.015	0.775	50,000	$2.32 \times 10^{-3}$	$6.71 \times 10^{-4}$
11	0.010	0.775	50,000	* $1.00 \times 10^{-3}$	...
12	0.040	0.830	30,000	$1.18 \times 10^{-2}$	...
13	0.025	0.830	30,000	$7.81 \times 10^{-3}$	...
14	0.020	0.830	30,000	$5.01 \times 10^{-3}$	...

*Note:* In the case where only one satellite is formed,  $M_{\text{s,out}}$  represents its mass at the end of simulation; when a co-orbital satellite and/or a small moonlet on an outer orbit is also formed as the second largest body in the system, their masses are also included in  $M_{\text{s,out}}$  to facilitate comparison with other cases. In the case where two satellites are formed,  $M_{\text{s,in}}$  and  $M_{\text{s,out}}$  are the masses of satellites on the inner orbit and the outer orbit, respectively; in this case,  $M_{\text{s,in}}$  is obtained from the mass of the second satellite just after its rapid growth phase. The asterisks denote the cases where a co-orbital satellite was formed on the orbit of the primary satellite.